# Neural MPPT of Variable-Pitch Wind Generators With Induction Machines in a Wide Wind Speed Range

Maurizio Cirrincione, *Senior Member, IEEE*, Marcello Pucci, *Senior Member, IEEE*, and Gianpaolo Vitale, *Senior Member, IEEE*

***Abstract*—This paper proposes a maximum power point tracking (MPPT) technique for variable-pitch wind generators with induction machines (IMs), which can suitably be adopted in both the maximum power range and the constant-power range of the wind speed. To this aim, an MPPT technique based on the growing neural gas (GNG) wind turbine surface identification and corresponding function inversion has been adopted here to cover also the situation of variable-power region. To cope with the constant-power region, the blade pitch angle has been controlled on the basis of the closed-loop control of the mechanical power absorbed by the IM. The wind speed is then estimated in the constant-power region on the basis of the actual position of the blade pitch angle. The proposed methodology has been verified both in numerical simulation and experimentally on a properly devised test setup. In addition, a comparison between the proposed approach and the previously developed GNG-based MPPT has been performed on a real wind speed profile. Finally, the effect of the torsional stiffness of the mechanical transmission system has been analyzed.**

***Index Terms*—Induction machine (IM), maximum power point tracking (MPPT), neural networks, variable-pitch turbines, wind generator.**

## NOMENCLATURE

| | |
|---|---|
| $\mathbf{u^u_{sg}} = u_{\mathrm{sgd}} + j u_{\mathrm{sgq}}$ | Space vector of the grid-side inverter voltages in the grid voltage reference frame. |
| $\mathbf{u_{sg}} = u_{\mathrm{sgD}} + j u_{\mathrm{sgD}}$ | Space vector of the grid-side inverter voltages in the fixed frame. |
| $\mathbf{u^u_g} = u_{\mathrm{gd}} + j u_{\mathrm{gq}}$ | Space vector of the grid voltages in the grid voltage reference frame. |
| $\mathbf{u_g} = u_{\mathrm{gD}} + j u_{\mathrm{gQ}}$ | Space vector of the grid voltages in the fixed reference frame. |
| $\mathbf{i^u_{sg}} = i_{\mathrm{sgd}} + j i_{sgq}$ | Space vector of the grid-side inverter currents in the grid voltage reference frame. |
| $\mathbf{i_{sg}} = i_{\mathrm{sgD}} + j i_{\mathrm{sgQ}}$ | Space vector of the grid-side inverter currents in the fixed reference frame. |
| $\rho_s$ | Angle of the grid voltage space vector. |
| $u_{\mathrm{sgA}}, u_{\mathrm{sgB}}, u_{\mathrm{sgC}}$ | Grid-side inverter phase voltages. |
| $i_{\mathrm{sgA}}, i_{\mathrm{sgB}}, i_{\mathrm{sgC}}$ | Grid-side inverter phase currents. |
| $L, R$ | Interconnection series inductance and its parasitic resistance. |
| $\omega$ | Pulsation of the electrical grid. |
| $\mathbf{u_{sxy}} = u_{\mathrm{sx}} + j u_{\mathrm{sy}}$ | Space vector of the machine-side inverter voltages in the rotor flux reference frame. |
| $\mathbf{u_s} = u_{\mathrm{sD}} + j u_{\mathrm{sQ}}$ | Space vector of the machine-side inverter voltages in the stator reference frame. |
| $\mathbf{i_{sxy}} = i_{\mathrm{sx}} + j i_{\mathrm{sy}}$ | Space vector of the machine-side inverter currents in the rotor flux reference frame. |
| $\mathbf{i_s} = i_{\mathrm{sD}} + j i_{\mathrm{sQ}}$ | Space vector of the machine-side inverter currents in the stator reference frame. |
| $u_{\mathrm{sA}}, u_{\mathrm{sB}}, u_{\mathrm{sC}}$ | Machine-side inverter phase voltages. |
| $i_{\mathrm{sA}}, i_{\mathrm{sB}}, i_{\mathrm{sC}}$ | Machine-side inverter phase currents. |
| $t_e$ | Electromagnetic torque. |
| $\boldsymbol{\psi_r}$ | Rotor flux linkage space vector. |
| $\rho_r$ | Angle of the rotor flux linkage space vector. |
| $p$ | Number of pole pairs. |
| $\omega_{\mathrm{mr}}$ | Machine speed (in mechanical angles). |
| $\omega_{\mathrm{m}}$ | Electric speed of the rotor flux linkage. |
| $\omega_T$ | Wind turbine speed. |
| $P_m$ | Turbine mechanical power. |
| $P$ | Generated electric active power. |
| $Q$ | Generated electric reactive power. |
| $C_p$ | Performance power coefficient of the turbine. |
| $C_T$ | Performance torque coefficient of the turbine. |
| $\rho$ | Air density. |
| $A$ | Turbine swept area. |
| $v$ | Wind tangential speed. |
| $\lambda$ | Tip speed ratio of the rotor blade tip speed. |
| $\beta$ | Blade pitch angle. |
| $n$ | Gear ratio. |

All variables with the subscript "ref" are reference quantities.

Manuscript received February 27, 2012; revised May 30, 2012; accepted June 6, 2012. Date of publication January 25, 2013; date of current version March 15, 2013. Paper 2012-IPCC-098.R1, presented at the 2011 IEEE Energy Conversion Congress and Exposition, Phoenix, AZ, USA, September 17–22, and approved for publication in the IEEE TRANSACTIONS ON INDUSTRY APPLICATIONS by the Industrial Power Converter Committee of the IEEE Industry Applications Society.

M. Cirrincione is with the Université Technologique de Belfort Montbeliard, 90010 Belfort, France (e-mail: m.cirrincione@ieee.org).

M. Pucci and G. Vitale are with the Institute of Intelligent Systems for Automation (ISSIA-CNR), 90128 Palermo, Italy (e-mail: marcello.pucci@ieee.org; gianpaolo.vitale@ieee.org).

Color versions of one or more of the figures in this paper are available online at http://ieeexplore.ieee.org.

Digital Object Identifier 10.1109/TIA.2013.2242817

## I. Introduction

WIND generation units with induction machines (IMs), interfaced with the power grid by a back-to-back inverter topology and supported by a vector control on both the machine-side and grid-side inverters, are among the most performing solutions to properly control the electromechanical power conversion with minimum impact on the grid [1], [2]. Additional performance in the generable power can be achieved by integrating the converter control with maximum power point tracking (MPPT) techniques [3], many of which are based on perturb and observe (P&O) methods [4]–[7]. Most of the techniques in literature are, however, devised only for fixed-pitch wind turbines, and they cannot be easily extended to variable-pitch turbines. According to the variations of the wind speed, the typical operation of a wind generator presents the following working regions [8]:

I) below cut-in speed (zero power);
II) maximum generable power (MPPT);
III) constant rated power;
IV) above cutoff speed (generator shut down).

Only variable-pitch wind turbines can work acting on the blade pitch angle in the constant rated power region at rated torque. In this sense, a proper modeling and simulation of blade pitch angle actuators is presented in [9]. Blade pitch angle control is therefore typically carried out in the constant-power region, while in the maximum power region the pitch angle is usually set to zero or a very small value to exploit the turbine optimally as proposed in [10], where, however, the adopted control technique of the pitch angle is not described. In [11] and [12], fuzzy controllers are used to manage the pitch angle. In [13], a blade pitch angle adaptive controller with a self-tuning regulator is presented, whose controlled variable is the generated power. A similar approach has been followed in [14], where either proportional integrals (PIs) with gain scheduling or fuzzy controllers are proposed. Another approach has been followed in [15], where different values of the pitch angle are selected on the basis of the current values of wind and machine speeds. An approach similar to that proposed here has been proposed by [16], which presents two neural pitch angle controllers, based on the back-propagation (BPN) algorithm. It should be noted that all of the aforementioned approaches imply the instantaneous knowledge of the wind speed, which is not an easy task even with an anemometer embedded in the turbine. Moreover, most papers present results only in numerical simulations without any experimental validation. This paper is an improvement of [3] and [17] and proposes an MPPT technique based on the growing neural gas (GNG) network, which can suitably be adopted in both the maximum power range and the constant-power range. To this aim, the MPPT technique based on the GNG identification of the wind turbine surface with the corresponding function inversion presented in [3] has been adopted to cope with the maximum power region. In [17], the GNG has been used to estimate the wind speed even in the constant-power region; to do that, the working space of the data—composed of the turbine angular speed, the wind speed, and the turbine torque—had been augmented (from 3 to 4), including also the blade pitch angle. This led up to an increase of the computational burden of the MPPT and the necessity to use the GNG in a recurrent form, with the estimated wind speed fed back and processed to compute the pitch angle to be given at the input of the GNG itself. The increase of the space state of the data, however, results in a reduction of the accuracy in the wind speed estimation and correspondingly in the computation of the correct value of the pitch angle. To cope with these last two issues, the solution proposed here has been devised. Unlike [17], here the GNG network has been used only in the maximum power region, thus reducing the working space of the data (maintained at 3) and, consequently, the computational demand of the GNG implementation. To cope with the constant-power region, the blade pitch angle has been controlled on the basis of the closed-loop control of the mechanical power absorbed by the IM from the turbine, whose reference is set to the machine rated power. The wind speed is then estimated in the constant-power region by using the information of the actual position of the blade pitch angle on the basis of a prestored function. The main advantage with respect to [17] is the significant reduction of the computational burden of the MPPT algorithm and a better control in the constant-power region. It should be noted that, differently from all of the aforementioned described methods, the approach proposed here does not need any wind speed measurement since its estimation is embedded in the methodology itself. Moreover, unlike many other works in the area, this methodology has been verified both in numerical simulation and experimentally on a properly devised test setup. In addition, a comparison between the proposed approach and the previously developed GNG-based MPPT has been performed on a real wind speed profile. Finally, the effect of the torsional stiffness of the mechanical transmission drive system has been analyzed.

## II. Wind Turbine Emulator With Variable Pitch

In the proposed test setup, the wind turbine has been emulated experimentally by a torque-controlled permanent magnet synchronous motor (PMSM) drive, whose speed-torque characteristic instantaneously reproduces the one of a real wind turbine. The model of the emulated turbine is described in the following. The power generated by a wind turbine can be written as [18]

$$P_m = C_p(\lambda, \beta)\frac{\rho A}{2}v^3 \tag{1a}$$

where $P_m$ is the mechanical power of the turbine in watts, $C_p$ is the power performance coefficient of the turbine, $\rho$ is the air density in kilograms per cubic meter, $A$ is the turbine swept area in cubic meter, $v$ is the wind speed in meters per second, $\lambda$ is the tip speed ratio defined as the ratio between the rotor blade tip and the speed of the wind

$$\lambda = \frac{\omega_T R}{v} \tag{1b}$$

where $\omega_T$ is the turbine angular speed and $R$ is the turbine radius, $\beta$ is the blade pitch angle in degrees

$$C_p(\lambda, \beta) = c_1\left(\frac{c_2}{\lambda_i} - c_3\beta - c_4\right)e^{\frac{-c_5}{\lambda_i}} + c_6\lambda \tag{1c}$$

TABLE I
WIND TURBINE PARAMETERS

| | |
|---|---|
| $R$ [m] | 2.5 |
| $\lambda_{opt}$ | 7 |
| $C_{pmax}$ | 0.45 |
| $n$ | 4,86 |
| Generator rated power [kW] | 5.5 |
| Generator rated speed [rad/s] | 150 |

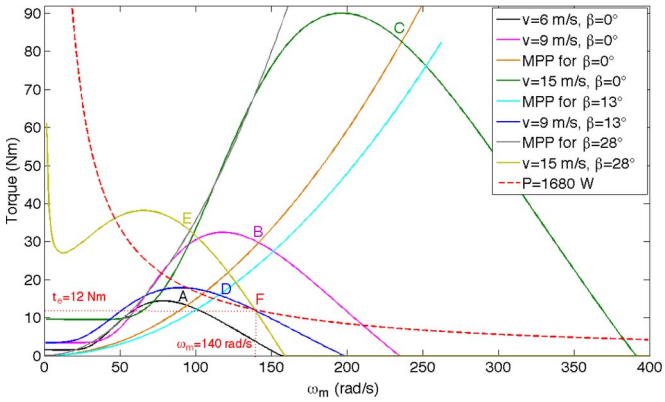


Fig. 1. Wind turbine torque versus speed characteristics for different free wind speeds and pitch angles.

with

$$\frac{1}{\lambda_i} = \frac{1}{\lambda + 0.08\beta} - \frac{0.035}{\beta^3 + 1} \tag{1d}$$

and

$$c_1 = 0.5176,\ c_2 = 116,\ c_3 = 0.4,\ c_4 = 5,\ c_5 = 21,\ c_6 = 0.0068.$$

The torque produced by the turbine can be computed as

$$T_T = P_m/\omega_T = C_T(\lambda, \beta)\frac{\rho\pi R^3}{2}v^2 \tag{1e}$$

where the torque coefficient of the turbine is defined as $C_T(\lambda, \beta) = C_P(\lambda, \beta)/\lambda$. Remark that both the turbine speed and the torque should be converted into the machine speed range on the basis of the gear ratio $n$ since $\omega_T' = \omega_T n = \omega_m$ and $T_T' = T_T/n$. The adopted turbine model parameters are shown in Table I, taken from [19]. Fig. 1 shows the torque versus speed characteristics of the emulated wind turbine, obtained for different values of the wind tangential speed $v$ (6, 9, and 15 m/s) and pitch angles $\beta$ (0°, 13°, and 28°), as well as the maximum power point (MPP) curves for each value of $\beta$. This figure also shows how the MPP curves change with the variation of the pitch angle $\beta$ as well as the hyperbola describing the constant rated power of the generator ($P_{\rm rat} = 1680$ W). These sets of curves show that, below a threshold wind speed (almost equal to 6 m/s for the adopted turbine), the MPPs correspond to a generated power lower than the rated one of the generator (points A in Fig. 1). On the contrary for $v = 9$ m/s (15 m/s), if the pitch angle control is not activated, the MPP corresponds to a generated power much higher than the rated one (points B and C in Fig. 1); for such wind speeds, even if the pitch angle is increased, respectively, to 13° and 28°, the MPP still lies above the rated power of the generator (points D and E in Fig. 1).

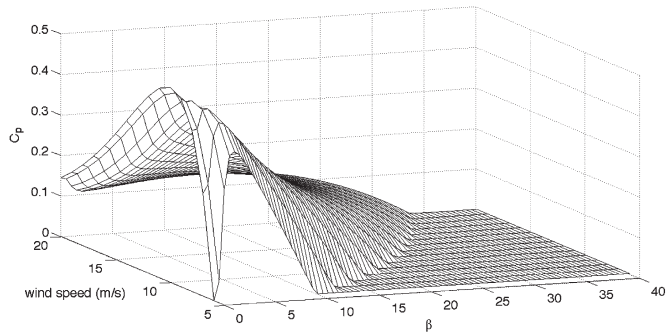


Fig. 2. Surface of $C_p$ versus wind speed and $\beta$.

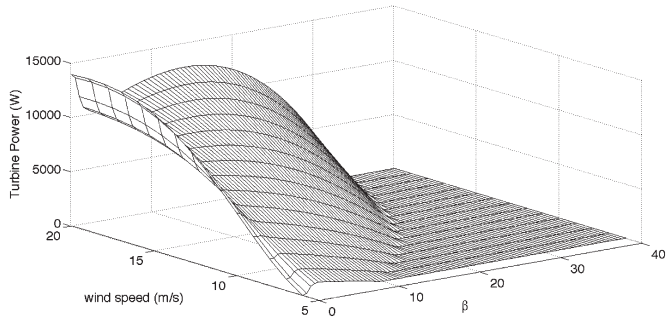


Fig. 3. Surface of the power versus wind speed and $\beta$.

This means that, in such working conditions, the system should be made to work at the generator rated power, i.e., at rated torque (12 N · m) and speed (140 rad/s), as shown in point F of Fig. 1. Fig. 2 shows the surface of $C_p$ versus $v$ and $\beta$, and Fig. 3 shows the surface of the turbine power versus $v$ and $\beta$, both drawn at the machine rated speed. In these figures, a highly nonlinear relationship of the turbine power and $C_p$ with respect to the wind speed $v$ and the pitch angle $\beta$ is apparent, which demands a complex control technique of the pitch angle $\beta$.

## III. CONTROL TECHNIQUE

The control system of the proposed wind generator is composed of three separate control systems: 1) a field-oriented control (FOC) for the induction generator; 2) a voltage-oriented control (VOC) for the grid-connected inverter; and 3) an MPPT algorithm including the control system for the blade pitch actuator.

### A. Machine-Side Converter With FOC

Since the wind turbine provides a torque which quickly changes with the wind speed, a high-performance control technique of the IM has been chosen, particularly the FOC [20]. In the adopted FOC scheme (Fig. 4), current control is performed in the rotor-flux-oriented reference frame. The dc link control is provided by the grid-side inverter. On the direct axis $(x)$, a flux control loop commands the direct current loop, and a voltage control loop commands the flux loop to permit the drive to work automatically in the field-weakening region by maintaining constant the product of the rotor flux amplitude and the absolute value of the rotor speed. On the quadrature axis $(y)$, a speed loop controls the quadrature current loop. The

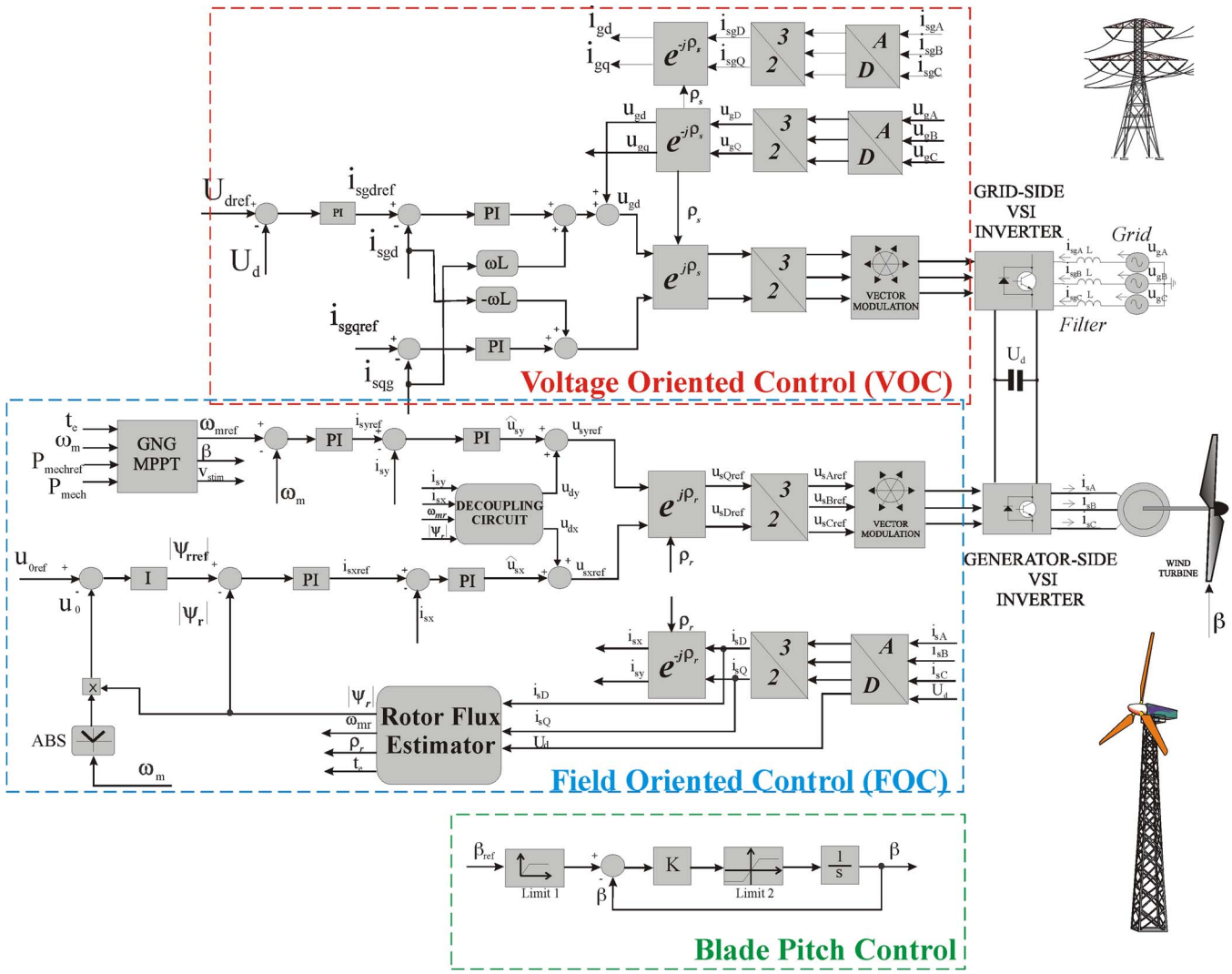


Fig. 4. Block diagram of the control system of the wind generation unit.

reference speed of the machine corresponding to the maximum power generable from the system at a given wind speed is retrieved by the GNG-based MPPT technique (described in Section IV). All controllers used in the control loops are proportional integral (PI) type. An asynchronous space vector pulsewidth modulation (SV-PWM) with $f_{\mathrm{PWM}} = 5$ kHz has been used to command the inverter. This modulation technique has been implemented by software on the same DSP on which the FOC runs. The use of such a control scheme permits the drive to follow the speed reference with high performance and to provide the torque required by the wind turbine, which is a nonlinear function of the speed of the machine itself, as well as to operate in the field-weakening region when the turbine speed increases.

### B. Grid-Side Converter With VOC

Grid-side converter control has been performed on the basis of a high-performance technique: VOC [1]. VOC is based on the idea of instantaneously decoupling the direct $(d)$ and quadrature $(q)$ components of the injected current, working in the grid voltage vector reference frame. Since the target here is to control directly the dc link voltage, the control scheme has been slightly modified by adding another control loop for the dc link voltage, which outputs the direct reference current. The quadrature current reference is always set to zero so that the reactive power flow with the grid can be kept to zero. Also, in this case, an asynchronous SV-PWM technique with an $f_{\mathrm{PWM}} = 5$ kHz has been adopted.

### C. Pitch Angle Control

The adopted wind turbine emulator, based on a torque-controlled PMSM drive, experimentally emulates a variable-pitch turbine, including the dynamics of the blade pitch angle actuator. Blade pitch control is primarily used to limit the aerodynamic power above rated wind speed in order to keep the turbine shaft torque within its design limits. The inertia of the blades rotated by the actuator is large, and so the pitch actuator generally has limited dynamical capabilities. Its dynamics is nonlinear with saturation limits on pitch angle (usually from $-3^\circ \div 90^\circ$) and pitching speed (around $8^\circ \div 10^\circ$ s$^{-1}$). These are the limits adopted in the emulated system. The configuration based on a closed loop structure with a saturation of the pitch

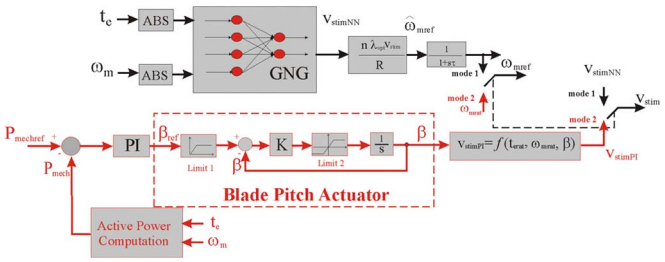


Fig. 5. Block diagram of the MPPT technique in modes 1 and 2.

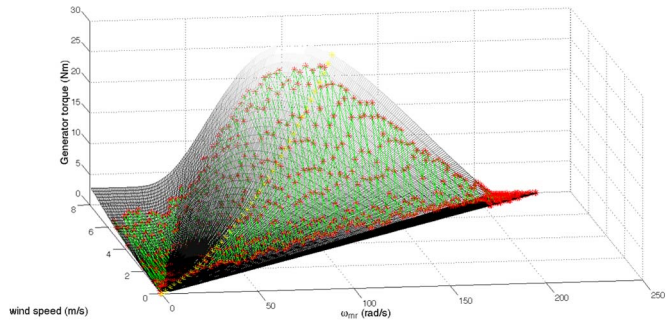


Fig. 6. Distribution of the neurons and links of GNG on the wind turbine surface.

angle and the limitation of its rate has been adopted here (see Fig. 4). Thus, given a reference value of the blade pitch angle $\beta_{\rm ref}$, the dynamic behavior of the blade pitch actuators has been modeled as a first-order system with a gain $K$ and two saturation blocks, one limiting the maximum value achievable by the pitch angle and one limiting its rate of change [9]. Parameter $K$ is a softness coefficient, acting when the limit is approaching. In particular, the lower the value of $K$, the slower the pitch angle approaches its reference when it is in its proximity.

## IV. GNG-Based MPPT for Variable-Pitch Wind Turbines

The basic idea is to have a unique MPPT system, permitting the system to work properly both in the maximum power region (low wind speed) and in the constant rated power region (high wind speed). To this aim, the MPPT technique based on the GNG [21]–[23] identification of the wind turbine surface and corresponding function inversion [3] has been further improved here to include the operation in the constant rated power region. The wind generator has been therefore assumed to work in two operating modes, called, respectively, modes 1 and 2, in accordance with the value of the wind speed (lower or higher than the threshold value of 6 m/s). The switching between modes 1 and 2 occurs when the estimated wind speed is higher than a threshold (6 m/s in this case, but it depends on the machine and turbine ratings). Fig. 5 shows the block diagram of the proposed MPPT technique, where a switch commutates from mode 1 to mode 2 and *vice versa*.

### A. Mode 1

In this mode, the target is to make the machine work at the speed corresponding to the maximum power extractable from the wind turbine. In this case, the MPPT algorithm works exactly as in [3]. It is operated when the estimated wind speed is below the threshold. In this case, the generator reference speed $\omega_{\rm mrref}$ can be computed on the basis of the following expression:

$$\omega_{\rm mrref} = n v_{\rm stim} \lambda_{\rm opt} / R \tag{2}$$

where $\lambda_{\rm opt}$ is the optimal value of the tip speed ratio, which is a known quantity and is dependent on the characteristics of the turbine, and $v_{\rm stim}$ is the estimated wind speed. For stability reasons, the optimal generator reference speed is not directly provided to the machine control system but is filtered by a first-order transfer function with time constant $\tau$ to avoid instability phenomena of the whole control system, as explained in [3].

The turbine model in Section II has been used to create the complete training set of data. This relationship has then been learned offline by a GNG network [21]–[23] developed by the authors in Matlab–Simulink environment (for the description of the adopted GNG algorithm, see [3]). A GNG with a maximum number of 800 neurons has been used, which does not imply a significant computational burden, since it requires only a storage of a $800 \times 3$ matrix in the memory of the DSP. After training, the GNG has been used online by exploiting the turbine characteristic function to be inverted. It should be noted that the function inversion capability is one of the key issues by which this neural network is suitable for this application, whereas the classic multilayer perceptron trained by the BPN is not able to perform this task. Fig. 6 shows the neurons created by the GNG (red) with the corresponding links (green) after training.

### B. Mode 2

Mode 2 occurs when the wind speed is above the threshold of 6 m/s. In this mode, the target is to limit the maximum generable power to the rated power of the machine, by making it work at its rated speed and torque. In mode 2, the mechanical power absorbed by the IM $P_{\rm mech}$ is closed-loop controlled to a constant value (typically set to its rated power). The reference power $P_{\rm mechref}$ is compared with the actual $P_{\rm mech}$, computed on the basis of the product of the estimated electromagnetic torque (corrected considering the friction torque) and measured machine speed, while the tracking error is processed by a PI controller. In particular, the mechanical power absorbed by the IM is computed as

$$P_{\rm mech} = t_e \omega_m \tag{3}$$

with

$$t_e = \frac{3pL_m}{2L_r} \psi_{rx} i_{sy} \tag{4}$$

where $\psi_{rx}$ and $i_{sy}$ are, respectively, the direct component of the rotor flux linkage and the quadrature component of the stator current, expressed in the rotor-flux-oriented reference frame. These variables are already all available from the machine control system.

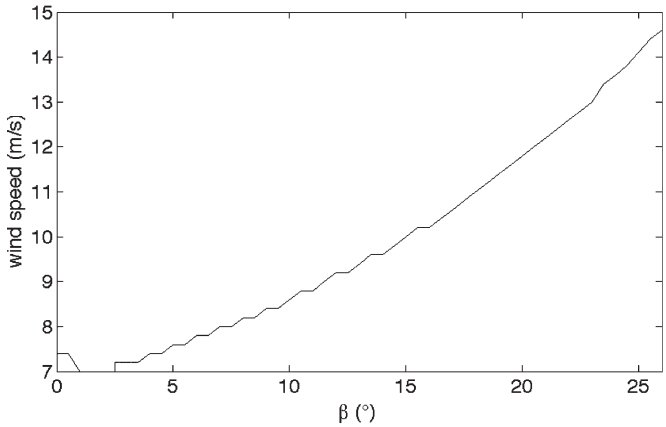


Fig. 7. Plot of the function $v_{stimPI} = f(\omega_{\mathrm{mrat}}, t_{\mathrm{erat}}, \beta)$.

TABLE II
PARAMETERS OF THE IM

| | |
|---|---|
| Rated power $P_{rated}$ [kW] | 2.2 |
| Rated voltage $U_{rated}$ [V] | 220 |
| Rated speed $\omega_{mrrat}$ [rad/s] | 140 |
| Rated frequency $f_{rated}$ [Hz] | 50 |
| Pole-pairs | 2 |
| Stator resistance $R_s$ [Ω] | 2.9 |
| Stator inductance $L_s$ [mH] | 223 |
| Rotor resistance $R_r$ [Ω] | 1.52 |
| Rotor inductance $L_r$ [mH] | 229 |
| 3-phase magnetizing inductance $L_m$ [mH] | 217 |
| Moment of inertia J [kg·m$^2$] | 0.0048 |

The output of the PI controller is the reference value of the pitch angle $\beta_{\mathrm{ref}}$, which is further provided to the blade pitch actuator control block, whose output is the actual value of the pitch angle $\beta$. In this way, the PI power controller selects the correct value of $\beta$, making the machine work at its rated power, as required. To estimate the wind speed in this working condition, the following direct relationship $v_{stimPI} = f(\omega_{\mathrm{mrat}}, t_{\mathrm{erat}}, \beta)$ is used, where $\omega_{\mathrm{mrrat}}$ and $t_{\mathrm{erat}}$ are, respectively, the machine rated speed and rated torque. This relationship, shown in Fig. 7 for the wind turbine under test, can be obtained on the basis of a preprocessing of the turbine model data and can be easily implemented on the DSP by a look-up table for experimentation.

## V. Test Setup

The employed test setup consists of two parts, respectively, the grid-side and machine-side parts. The grid-side part is composed of the following items:

1) an 8-kVA three-phase VSI;
2) a dSPACE card (DS1103) with a PowerPC 604e at 400 MHz and a floating-point DSP TMS320F240 for the control of the grid-side inverter;
3) an interconnection series inductance of 12 mH with a parasitic resistance of 0.9 Ω.

The machine-side part is composed of the following items:

1) a three-phase induction machine with parameters shown in Table II;
2) an 8-kVA three-phase VSI for the control of the machine-side inverter;

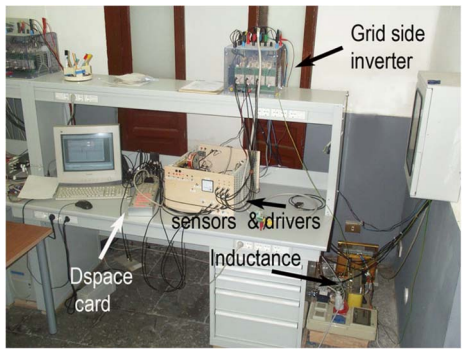


Fig. 8. Photograph of the test setup (grid-side inverter + interconnecting inductance).

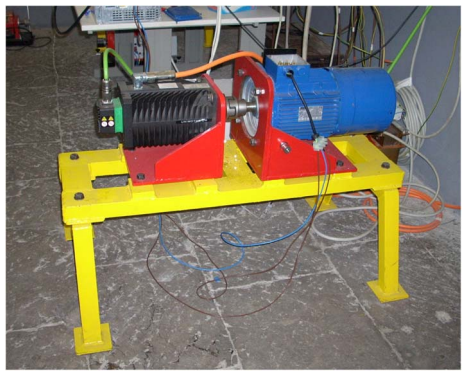

Fig. 9. Photograph of the test setup (induction generator + turbine emulator).

3) a brushless interior mounted permanent magnet machine drive for emulating the wind turbine;
4) a dSPACE card (DS1103) with a PowerPC 604e at 400 MHz and a floating-point DSP TMS320F240 for the control of the machine-side inverter.

Figs. 8 and 9 show two photographs of the test setup. Each DSP is dedicated to the FOC for the machine-side inverter control as well as the MPPT algorithm with the wind turbine model described in Section II, with the other to the VOC for grid-side inverter control. For computational reasons, each task has been performed by the DSP with a different timing: both the FOC and VOC (9 control loops) have been implemented at a sampling frequency of 10 kHz, while the MPPT is at a sampling frequency 100 times lower (100 Hz). The wind turbine model, having as inputs the wind speed (given by the user), the value of $\beta$, computed by the MPPT algorithm, and the machine rotational speed (given by the encoder), provides the turbine torque signal to a PMSM machine torque-controlled drive. In this way, the PMSM machine drive behaves exactly as the wind turbine for each value of the wind speed and machine speed.

## VI. Experimental Results

The GNG-based MPPT technique for the wind generation system with an IM and variable-pitch turbine has been experimentally implemented and verified on the test setup described in Section V. To show the goodness of the proposed MPPT

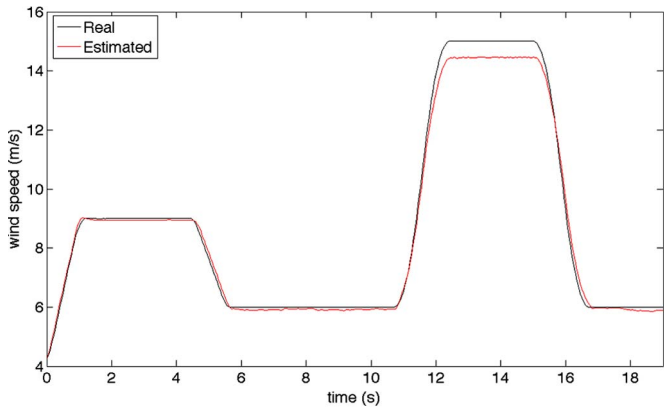


Fig. 10. Real and estimated wind speeds.

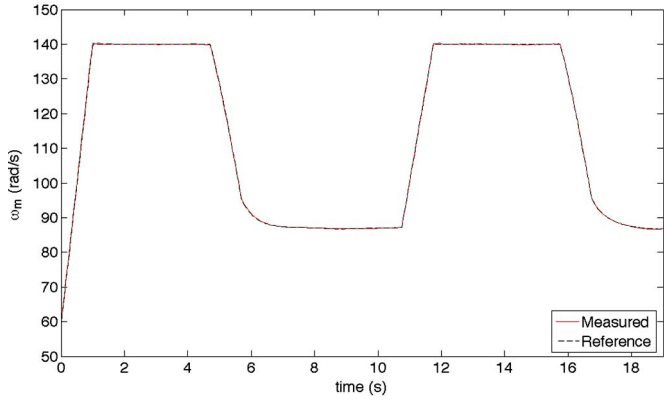


Fig. 11. Reference and measured machine speeds.

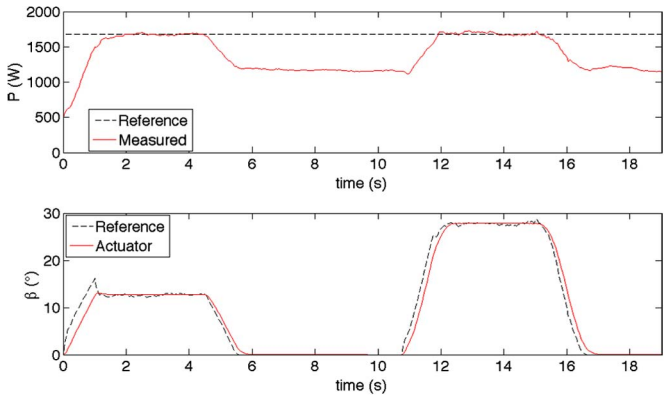


Fig. 12. Reference and actual values of the mechanical power $P_{\mathrm{mech}}$ and the pitch angle $\beta$.

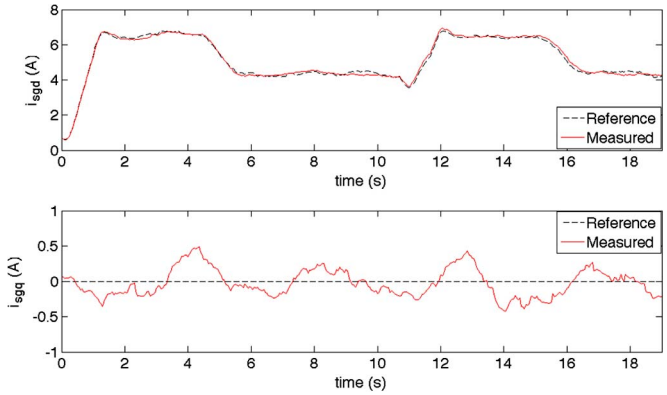


Fig. 13. Grid-side $i_{sd}$ and $i_{sq}$ currents.

technique, the following experimental test has been made, including a set of sudden transitions from low to high wind speed and *vice versa*. The wind generation system, initially working in steady state at a wind speed of 4 m/s, has been given at time $t = 0$ s a step variation of the wind speed to 9 m/s, then to 6 m/s, to 15 m/s, and, finally, to 6 m/s. Fig. 10 shows the real wind speed and the corresponding one estimated by the system, respectively, GNG network in the maximum power region and direct relationship in the constant-power region. It should be noted that the estimated speed converges properly to the real one for both low and high wind speeds, confirming the goodness of the proposed approach as far as wind speed estimation is concerned. Correspondingly, Fig. 11 shows the reference and measured machine speeds $\omega_m$ which, when the wind speed is below the threshold, are set to its optimal power value and, when the wind speed is above the threshold, are set to the rated speed of the machine (140 rad/s). As expected, the higher the wind speed, the higher the speed reference of the machine, limited to its rated value for high values of the wind speed. Fig. 12 upper plot shows the reference $(P_{\mathrm{mechref}})$ and actual $(P_{\mathrm{mech}})$ mechanical power absorbed by the machine. It can be observed that, below the wind threshold speed, the mechanical power of the machine is lower than the rated one, while above the threshold speed, it is correctly controlled to the rated power, as expected. Fig. 12 lower plot shows the reference and actual values of the pitch angle of the turbine. This value is controlled to zero in the maximum power region and to a positive value in the constant-power region, as expected. Also in this case, the higher the wind speed, the higher the value of the pitch angle necessary to maintain constant the electrical active power of the machine. Remark that the pitch angle variation is commanded by the control system before the machine speed gets its rated value: this quickly prevents the machine power from overcoming the rated power because of the fast wind speed variation. Fig. 13 shows the grid-side reference and measured current components ($i_{sd}$ and $i_{sq}$). Fig. 14 shows the corresponding waveforms of the active $(P)$ and reactive $(Q)$ powers exchanged by the system with the power grid. They show that both the $i_{sq}$ current and the reactive power $Q$ are controlled to zero, so no reactive power exchange with the power grid exists. On the contrary, at each increase of the wind speed, there corresponds an increase of both the $i_{sd}$ current and the active power $P$, in accordance with the higher generable power. In the constant-power region, the generated power is limited to a constant value lower than the rated power of the machine, being its mechanical power controlled to the rated value.

Fig. 15 shows the machine-side $i_{sx}$ and $i_{sy}$ reference and measured current reference. With regard to the machine currents $i_{sx}$ and $i_{sy}$, as expected, $i_{sx}$ remains constant, showing a constant magnetization of the machine, while $i_{sy}$ exhibits a variation of the amplitude at each variation of the wind speed. It could be noted in this particular case that the $i_{sy}$ component in the constant-power region, both for 9 m/s (13°) and 15 m/s (28°)

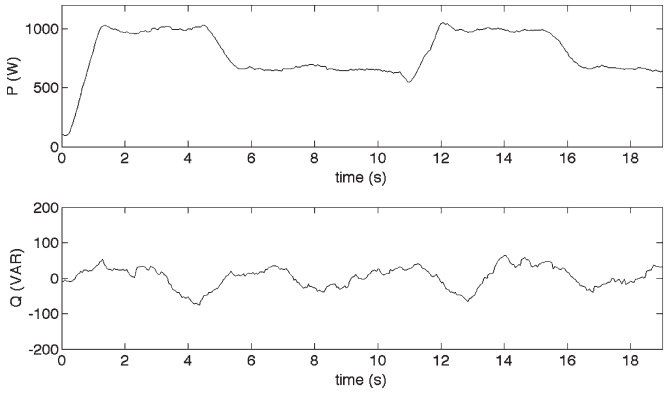


Fig. 14. Active $(P)$ and reactive $(Q)$ powers exchanged with the power grid.

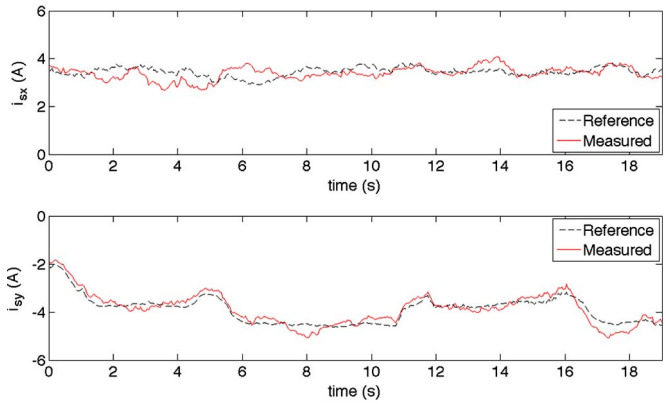


Fig. 15. Machine-side $i_{sx}$ and $i_{sy}$ currents.

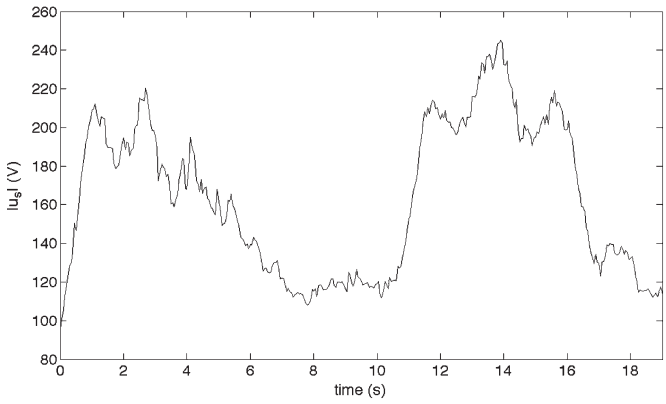


Fig. 16. Machine-side stator voltage $|\mathbf{u}_s|$ amplitude.

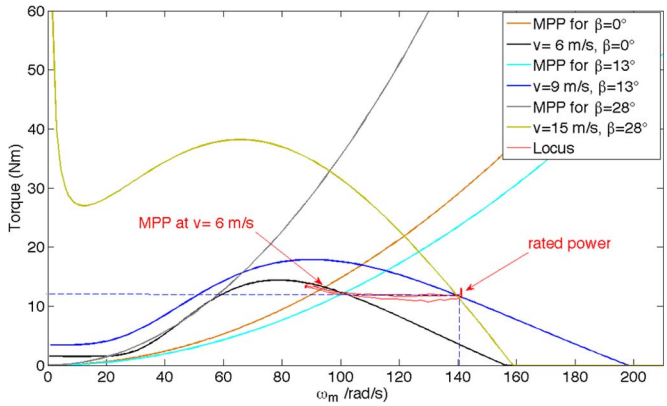


Fig. 17. Torque versus speed locus.

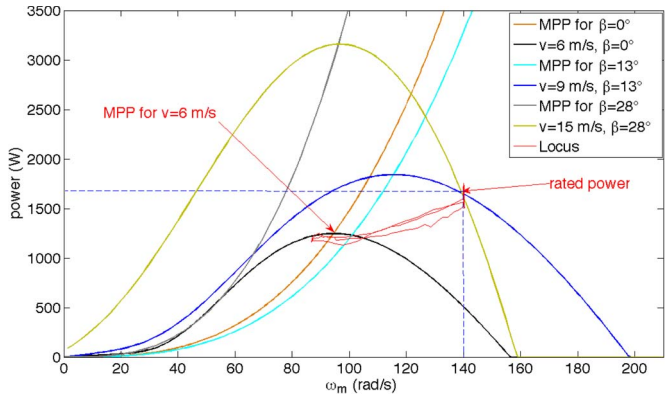


Fig. 18. Power versus speed locus.

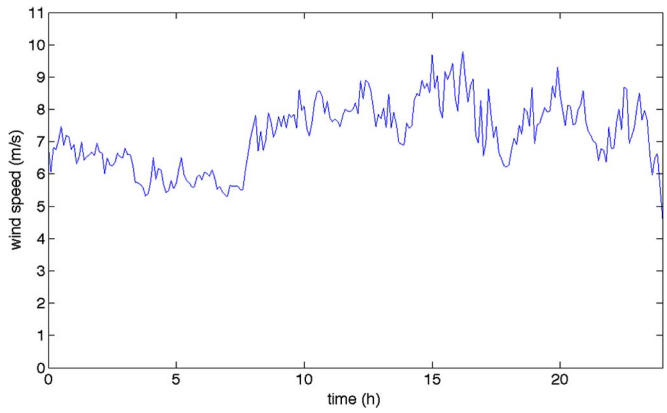


Fig. 19. Wind speed profile on a daily scale.

of wind speed, is almost equal or slightly lower than that at the threshold wind speed of 6 m/s, as confirmed by the steady-state torque characteristics in Fig. 1 (compare points A and F).

Fig. 16 shows the amplitude of the stator voltage space vector $|\mathbf{u}_s|$, as applied to the machine winding terminals during the aforementioned test. It can be observed that, the higher the wind speed and, consequently, the turbine torque, the higher the amplitude of the stator voltage, as expected, which is close to the rated one of the machine in correspondence of the constant-power working region (mode 2). Finally, Fig. 17 shows the "torque versus speed" characteristics of the turbine for different values of the wind speed and pitch angles as well as the steady-state maximum power curves and the transient "machine torque versus speed" locus drawn during the test. It should be noted that the steady-state points of this locus lie on the corresponding turbine characteristics as well as on the maximum power trajectory for wind speeds below the rated power of the machine, while they lie in correspondence of the rated values of the torque and the speed for wind speeds above the rated power of the machine. This is confirmed by the power versus speed locus in Fig. 18, showing clearly that the locus of the power lies in steady state on the MPPs in the variable-power region and on the constant (rated) power in the constant-power region. These two last figures confirm the effectiveness of the proposed approach.

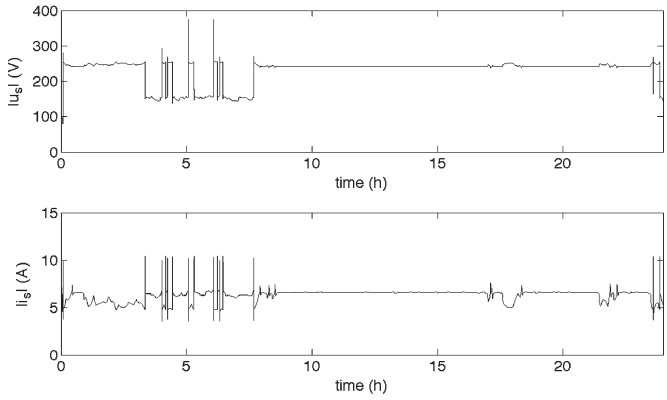


Fig. 20. Machine-side stator voltage and current $|\mathbf{u}_s|$ and $|\mathbf{i}_s|$ amplitudes.

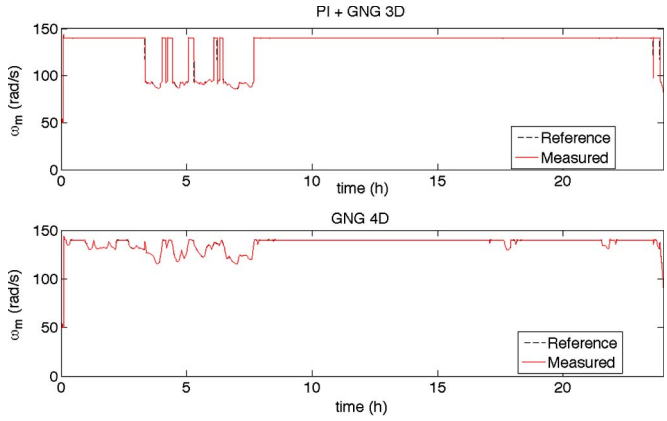


Fig. 21. Reference and measured machine speeds.

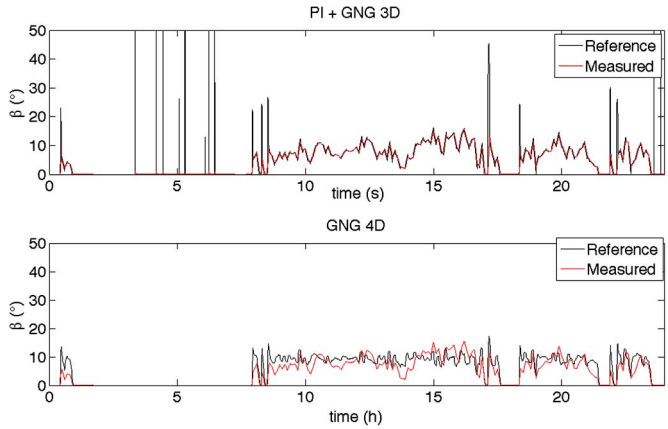


Fig. 22. Reference and actual values of the pitch angle $\beta$.

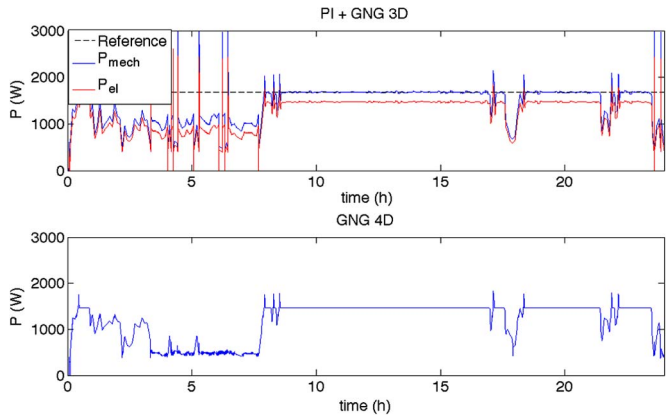


Fig. 23. Generated active power.

### A. Verification on a Real Wind Profile

The proposed GNG-based MPPT technique, identified in the following figures as PI + GNG 3-D, suitable for both the variable-power and constant-power working regions, has been verified also on a real wind speed profile. In particular, a real wind speed profile, measured in a location in Sicily, Italy, on a daily scale has been used. A wind profile with fast wind gusts at very high speed (in average above 6 m/s) has been selected to verify the system in continuous transitions between the variable-power and constant-power regions. This methodology has been further compared, on the same real wind speed profile, with the previously developed neural-based MPPT for both the variable-power and constant-power working regions [17], identified in the following figures as GNG 4-D. Fig. 19 shows the adopted wind speed profile during 24 h. Fig. 20 shows the corresponding amplitudes of the stator voltage and current space vectors, $|\mathbf{u}_s|$ and $|\mathbf{i}_s|$, as obtained with the PI + GNG 3-D. It can be observed that, the higher the wind speed and, consequently, the turbine torque, the higher the amplitudes of the stator voltage and current, as expected, which are almost constant and close to the rated ones of the machine in correspondence of the constant-power working region (mode 2). Fig. 21 shows the reference and measured machine speeds, as obtained with the PI + GNG 3-D and the GNG 4-D MPPTs. It can be observed that, when the wind speed is below the power threshold level, the machine speed is regulated to track the maximum available power; when the wind speed is above the power threshold level, the machine speed is limited to the rated one to track the rated power of the machine. There are slight differences in the curves obtained with both MPPTs, especially in the variable-power region, due to the better wind speed estimation accuracy performed by the GNG 3-D structure in comparison with the GNG 4-D. Fig. 22 shows the reference and actual values of the pitch angle $\beta$ with both MPPTs. The pitch angle is controlled to zero in the variable-power region and bigger than zero in the constant-power region, as expected. Even in this case, slight differences in the pitch commands are observable in the constant-power region. Finally, Figs. 23 and 24 show the generated active power and energy with both MPPTs. As far as the PI + GNG 3-D is concerned, also the reference and estimated mechanical powers are shown. It can be observed that, below the wind threshold speed, the mechanical power is lower than the rated one. Above the threshold, it is controlled at the rated power, as expected. The comparison between the two MPPTs shows a slightly higher generated power with the PI + GNG 3-D than with the GNG 4-D, which is due, as explained previously, to the better accuracy in the estimation of the wind speed. This is confirmed by the energy curves, showing a capability of the PI + GNG 3-D to extract 29.4 kWh versus the 28.5 obtainable with the GNG 4-D. The PI + GNG 3-D permits extracting, on a daily scale, almost 3.15% more of energy than the GNG 4-D (Fig. 24).

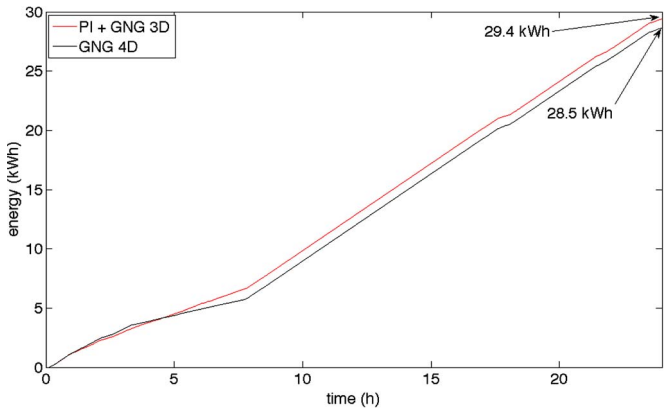


Fig. 24. Generated energy.

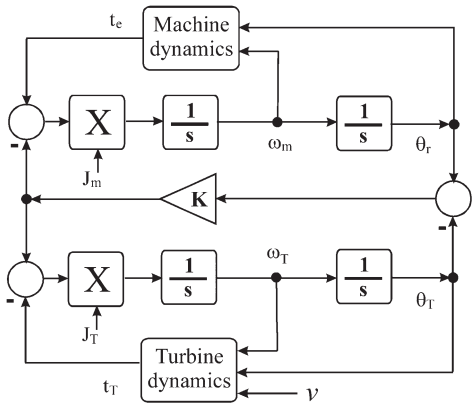


Fig. 25. Block diagram of the elastic two mass flexible shaft system.

### *B. Analysis of the Torsional Stiffness Effect of the Mechanical Transmission System*

Another important issue which has been studied is the effect of the torsional stiffness of the mechanical transmission drive system. The considered mechanical model representing the drive system dynamics is shown in Fig. 25. For the sake of simplicity, the transmission ratio of the gearbox has been considered unitary (as it is in the experimental test setup). It includes the turbine and machine dynamics plus their equivalent inertias ($J_T$ and $J_m$). The effect of a flexible shaft is represented by a torsional stiffness with constant $K$ supposedly located at the low speed side of the gearbox. The system has been initially tested with the value of $K = 3300$ N · m/rad equal to that of the adopted mechanical shaft present in the test setup (model Rotex Polynorm). The system has been tested under the same real wind speed profile in Fig. 19. Figs. 26 and 27 show, respectively, the turbine and machine speeds and the turbine, machine, and elastic torques during this test. It can be observed that both the machine and turbine speeds track the reference at steady state, with a slight overshoot of the turbine speed during fast transients (see the zoomed part of the graph). Correspondingly, the machine torque tracks the elastic and turbine ones at steady state, with the machine torque tracking the elastic one during fast transients, implying an overshoot of it with respect to the turbine one (see the zoomed part of the graph). However, no critical oscillations either of the speed or of the torque occur.

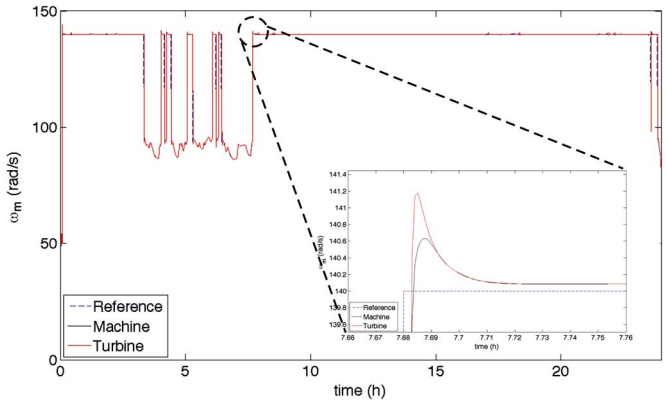


Fig. 26. Machine and turbine speeds with the two-mass flexible shaft system ($K$ of the real shaft).

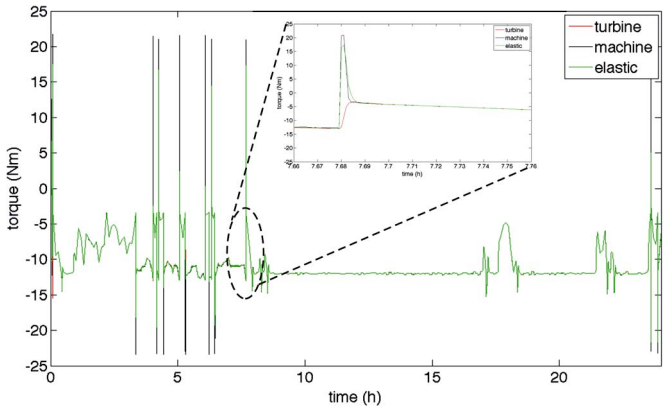


Fig. 27. Machine, turbine, and elastic torques with the two-mass flexible shaft system ($K$ of the real shaft).

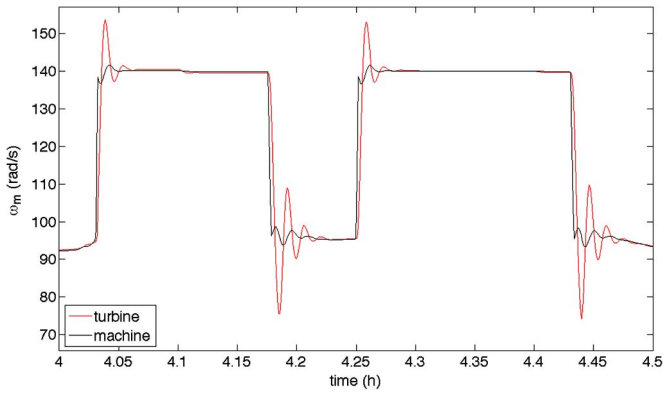


Fig. 28. Machine and turbine speeds with the two-mass flexible shaft system ($K$ equal to 1/100 of the real shaft).

Afterward, the system has been tested with the value of $K = 330$ N · m/rad, corresponding to 1/100 of that of the real shaft. Figs. 28 and 29, respectively, show the turbine and machine speeds and the turbine, machine, and elastic torques during this test (only a zoom of the entire graph is shown). Both figures show that, even reducing significantly the value of $K$, either the speed or the torque oscillations are significantly increased, without, however, becoming critical; the system in any case still works properly at steady state.

Finally, some considerations on the advantages of the proposed approach should be made from the commercial point of view. First, one of the pros is the lack of any anemometer for

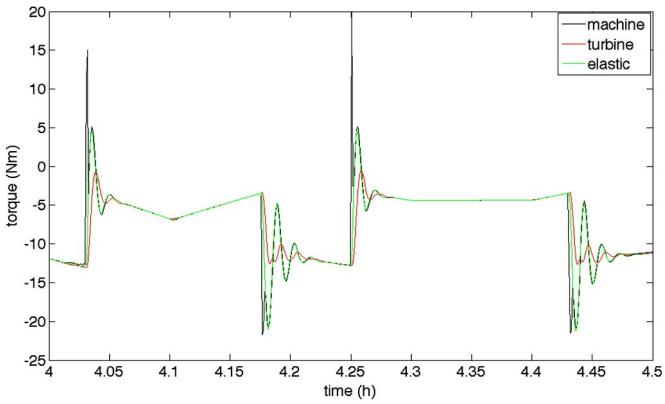


Fig. 29. Machine, turbine, and elastic torques with the two-mass flexible shaft system ($K$ equal to 1/100 of the real shaft).

measuring the wind speed, increasing the system reliability and making it cheaper. Then, the hardware implementation of the GNG network (recalling phase) is not particularly cumbersome from the computational point of view and is particularly suited for some hardware with parallel working structures, like FPGAs. The proposed MPPT ensures an immediate lock of the MPP, without oscillation typical of classical P&O algorithm; in this way, the harvested energy is increased especially for low values of the wind speed. Furthermore, the integration of the GNG-based MPPT with the PI control ensures a proper working of the generator in a wide range of wind speed, with a proper performance in the transitions between the MPP and constant-power regions. Finally, the GNG network initial offline training can be performed for different turbine designs directly with help either of the finite-element analysis or of the experimental analysis in the wind tunnel.

## VII. Conclusion

This paper has proposed an MPPT technique for variable-pitch wind generators with IMs, which can suitably be adopted in both the maximum power range and the constant power range of the wind speed. To this aim, an MPPT technique based on the GNG identification of the wind turbine surface and the corresponding function inversion has been adopted here to cover the situation of variable-power region. To cope with the constant-power region, the blade pitch angle has been controlled on the basis of the closed-loop control of the mechanical power absorbed by the IM, whose reference is set to its rated power. The wind speed is then estimated in the constant-power region on the basis of the actual position of the blade pitch angle. The proposed methodology has been verified both in numerical simulation and experimentally on a properly devised test setup. Results show a good behavior of the system, permitting the maximum generable power to be extracted at low wind speeds and making the system work at the machine rated power at high wind speed with proper control of the blade pitch actuators. Finally, a comparison between the proposed approach and the previously developed GNG-based MPPT has been performed on a real wind speed profile, showing that the proposed approach permits the production of 3.15% more of energy on a daily scale.

## References

[1] M. P. Kazmierkowski, R. Krishnan, and F. Blaabjerg, *Control in Power Electronics*. London, U.K.: Academic, 2002.

[2] M. Godoy Simões and F. A. Farret, *Alternative Energy Systems: Design and Analysis With Induction Generators*, 2nd ed. Boca Raton, FL, USA: CRC Press, 2002.

[3] M. Cirrincione, M. Pucci, and G. Vitale, "Growing neural gas (GNG) based maximum power point tracking for high performance VOC–FOC based wind generator system with induction machine," *IEEE Trans. Ind. Appl.*, vol. 47, no. 2, pp. 861–872, Mar./Apr. 2011.

[4] R. Datta and V. T. Ranganathan, "A method of tracking the peak power points for a variable speed wind energy conversion system," *IEEE Trans. Energy Convers.*, vol. 18, no. 1, pp. 163–168, Mar. 2003.

[5] R. Datta and V. T. Ranganathan, "A method of tracking the peak power points for a variable speed wind energy conversion system," *IEEE Power Eng. Rev.*, vol. 22, no. 10, p. 57, 2002.

[6] R. Datta and V. T. Ranganathan, "Variable-speed wind power generation using doubly fed wound rotor induction machine—A comparison with alternative schemes," *IEEE Trans. Energy Convers.*, vol. 17, no. 3, pp. 414–421, Sep. 2002.

[7] R. Datta and V. T. Ranganathan, "Variable-speed wind power generation using a doubly fed wound rotor induction machine: A comparison with alternative schemes," *IEEE Power Eng. Rev.*, vol. 22, no. 7, p. 52, 2002.

[8] B. Neammanee, S. Sirisumranukul, and S. Chatratana, "Control performance analysis of feedforward and maximum peak power tracking for small- and medium-sized fixed pitch wind turbines," in *Proc. 9th ICARCV*, Dec. 5–8, 2006, pp. 1–7.

[9] Y. El-Tous, "Pitch angle control of variable speed wind turbine," *Amer. J. Eng. Appl. Sci.*, vol. 1, no. 2, pp. 118–120, 2008.

[10] E. Muljadi and C. P. Butterfield, "Pitch-controlled variable-speed wind turbine generation," in *Conf. Rec. IEEE IAS Annu. Meeting*, Phoenix, AZ, USA, Oct. 3–7, 1999, pp. 323–330.

[11] M. Perales, J. Ptrez, F. Barrero, J. L. Mora, E. GalvBn, J. M. Carrasco, L. G. Franquelo, D. de la Cruz, L. Fernandez, and A. Zazo, "Fuzzy logic control of a variable speed, variable pitch wind turbine," in *Proc. IEEE IECON*, Nov. 29–Dec. 3 1999, vol. 2, pp. 614–618.

[12] M. A. M. Prats, J. M. Carrasco, E. Galvàn, J. A. Sànchez, L. G. Franquelo, and C. Batista, "Improving transition between power optimization and power limitation of variable speed, variable pitch wind turbines using fuzzy control," in *Proc. IEEE IECON*, Oct. 22–28, 2000, vol. 3, pp. 1497–1502.

[13] T. Senjyu, R. Sakamoto, N. Urasaki, H. Higa, K. Uezato, and T. Funabashi, "Output power control of wind turbine generator by pitch angle control using minimum variance control," *Elect. Eng. Jpn.*, vol. 154, no. 2, pp. 10–18, 2006.

[14] J. Zhang, M. Cheng, Z. Chen, and X. Fu, "Pitch angle control for variable speed wind turbines," in *Proc. 3rd Int. Conf. Elect. Utility DRPT*, Apr. 6–9, 2008, pp. 2691–2696.

[15] B. M. Nagai, K. Ameku, and J. Nath Roy, "Performance of a 3 kW wind turbine generator with variable pitch control system," *Appl. Energy*, vol. 86, no. 9, pp. 1774–1782, Sep. 2009.

[16] A. S. Yilmaz and Z. Özer, "Pitch angle control in wind turbines above the rated wind speed by multi-layer perceptron and radial basis function neural networks," *Exp. Syst. Appl.*, vol. 36, no. 6, pp. 9767–9775, Aug. 2009.

[17] M. Cirrincione, M. Pucci, and G. Vitale, "Growing neural gas based MPPT of variable pitch wind generators with induction machines," *IEEE Trans. Ind. Appl.*, vol. 48, no. 3, pp. 1006–1016, May/Jun. 2012.

[18] L. L. Freris, *Wind Energy Conversion System*. Englewood Cliffs, NJ, USA: Prentice-Hall, 1990.

[19] R. Leidhold, G. Garcia, and M. I. Valla, "Maximum efficiency control for variable speed wind driven generators with speed and power limits," in *Proc. IEEE IECON*, Seville, Spain, Nov. 5–8, 2002, pp. 157–162.

[20] P. Vas, *Sensorless Vector and Direct Torque Control*. Oxford, U.K.: Oxford Science, 1998.

[21] B. Fritzke, "Growing cell structures—A self-organizing network for unsupervised and supervised learning," *Neural Netw.*, vol. 7, no. 9, pp. 1441–1460, 1994.

[22] B. Fritzke, "Incremental learning of linear local mappings," in *Proc. ICANN*, Paris, France, 1995, pp. 217–222.

[23] B. Fritzke, "A growing neural gas network learns topologies," in *Advances in Neural Information Processing Systems 7*. Cambridge, MA, USA: MIT Press, 1995.

**Maurizio Cirrincione** (M'03–SM'10) received the "Laurea" degree in electrical engineering from the Polytechnic of Turin, Turin, Italy, in 1991 and the Ph.D. degree in electrical engineering from the University of Palermo, Palermo, Italy, in 1996.

Since 1996, he has been a Researcher at the Section of Palermo of the Institute of Intelligent Systems for Automation (ISSIA-CNR), Palermo. Since September 2005, he has been a Professor with the University of Belfort Mobeliard, Belfort, France. His current research interests are neural networks for modeling and control, system identification, intelligent control, and electrical machines and drives.

Prof. Cirrincione was awarded the prize "E.R.Caianiello" for the best Italian Ph.D. thesis on neural networks in 1997.

**Marcello Pucci** (M'03–SM'11) received the "Laurea" and Ph.D. degrees in electrical engineering from the University of Palermo, Palermo, Italy, in 1997 and 2002, respectively.

In 2000, he was a host student at the Institute of Automatic Control, Technical University of Braunschweig, Braunschweig, Germany, working in the field of control of ac machines, with a grant from the Deutscher Akademischer Austauscdienst—German Academic Exchange Service (DAAD). From 2001 to 2007, he was a Researcher at the Section of Palermo of the Institute of Intelligent Systems for Automation (ISSIA-CNR), Palermo, where he has been a Senior Researcher since 2008. He is a member of the Editorial Board of the *Journal of Electrical Systems*. His current research interests are electrical machines and drives, control of electrical drives, wind and photovoltaic generation systems, intelligent control, and neural network applications.

Dr. Pucci serves as an Associate Editor of the IEEE TRANSACTIONS ON INDUSTRY APPLICATIONS and IEEE TRANSACTIONS ON INDUSTRIAL ELECTRONICS.

**Gianpaolo Vitale** (A'04–M'06–SM'12) received the "Laurea" degree in electronic engineering from the University of Palermo, Palermo, Italy, in 1988.

From 1994 to 2001, he was a Researcher with the Institute of Intelligent Systems for Automation (ISSIA-CNR), Palermo, where he has been a Senior Researcher since 2002. He was a Professor of power electronics and applied electronics with the Engineering Faculty of Palermo from 1999 to 2007. He has been the Supervisor of a research project on electromagnetic compatibility of electric drives and of a research project on intelligent management of electric energy supplied by renewable sources. He serves as a reviewer for several journals and conferences. His current research interests are in the fields of power electronics and related problems of electromagnetic compatibility.

Prof. Vitale is a member of the IEEE Vehicular Technology Society, IEEE Industrial Electronics Society, and IEEE Electromagnetic Compatibility Society.